Journal of Materials Chemistry C

PAPER

View Article Online
View Journal | View Issue



Cite this: J. Mater. Chem. C, 2015, 3, 2291

# Synergetic effect of C*N^N/C^N^N coordination and the arylacetylide ligands on the photophysical properties of cyclometalated platinum complexes†

Wenting Wu,[ab] Xueyan Wu,[a] Jianzhang Zhao*[b] and Mingbo Wu*[a]

Received 18th October 2014
Accepted 15th December 2014

DOI: 10.1039/c4tc02358g

www.rsc.org/MaterialsC

Six coordinated Pt(II) complexes were prepared, in which the C*N^N or the C^N^N ligand were used to form the Pt(II) coordination center. For each coordination profile, three different arylacetylide ligands were used, *i.e.* naphthalenediimide (NDI), pyrenyl (Py) and naphthaleneimide (NI) acetylides. The electrochemical and the photophysical properties of the complexes were studied with steady-state and time-resolved absorption and emission spectroscopy, cyclic voltammetry and DFT calculations. The photostability and the photoluminescent properties of the complexes are finely tuned by the photoredox and photophysical properties of the arylacetylide ligands and the C*N^N/C^N^N Pt(II) coordination center. The triplet excited states of the complexes are an intraligand feature and the lifetime is long (90.1 μs). The photophysical properties of the complexes were rationalized with DFT calculations. The complexes were used as triplet photosensitizer for triplet–triplet annihilation upconversion. The upconversion quantum yield was up to 29.7%. The results are useful for future designing of Pt(II) complexes showing strong visible light-absorption, RT phosphorescence and long-lived triplet excited states.

## Introduction

Platinum(II) complexes have attracted considerable attention due to their fascinating photophysical properties such as tunable absorption/emission wavelength and feasibly derived molecular structures. These complexes have been widely used in electroluminescence and photoredox catalytic organic reactions,[1] photocatalytic hydrogen ($H_2$) production,[2] phosphorescent molecular probes,[3–5] singlet oxygen sensitization[6] and triplet–triplet annihilation upconversion.[7–10]

Recently, a great deal of effort has been devoted to developing C^N or C^N^N ligands to obtain a planar geometry of the Pt(II) coordination center with which the photoluminescence can be enhanced.[11–13] Different arylacetylide ligands were also used to enhance the visible-light-harvesting ability and prolong the lifetime of the triplet excited state.[8,9,14–19] Our group prepared N^N Pt(II) complexes with acetylide ligands based on Bodipy,[20] naphthalimide (NI),[21] naphthalenediimide (NDI),[22] pyrene (Py),[21] rhodamine,[23] fluorescein[24] and coumarin moieties.[25]

However, most studies on Pt(II) complexes are focused on the optimization of π-conjugation or simply introducing arylacetylide ligands. Actually, the geometry of the Pt(II) coordination center, charge transfer process (MLCT) and energy transfer process (intraligand energy transfer, IL ↔ MLCT) have a great synergic effect on the photophysical properties of Pt(II) complexes. A Pt(II) coordination center as a triplet spin convertor plays an important role in triplet photosensitizers due to efficient intersystem crossing ($^1$MLCT → $^3$MLCT). Furthermore, a charge transfer process and energy transfer process may compete with each other. It is highly desirable to develop molecular structure design rationales for Pt(II) complexes to tune the driving forces for charge transfer and energy transfer, when the geometry for the Pt(II) coordination center is fixed.

Organic fluorophores can absorb visible light, and their photoredox properties (driving forces for charge transfer) and their energy levels of emission and absorption can be finely modified by rational design and synthesis.[26] Herein we studied the aforementioned synergetic effect based on the C^N^N/C*N^N coordination protocol developed by Huo *et al.*[27] Six Pt(II) complexes with two different coordination ligands, *i.e.* a C*N^N with a five–six fused metallacycle or a C^N^N with a five–five fused metallacycle, were prepared. On the other hand, with different singlet/triplet state energy levels and redox properties, three different arylacetylide ligands based on Py, NI and NDI moieties were used for the construction of the Pt(II) complexes

[a]State Key Laboratory of Heavy Oil Processing, China University of Petroleum, Qingdao 266580, P. R. China. E-mail: wumb@upc.edu.cn; Fax: +86 532 8698 1787; Tel: +86 532 8698 3452

[b]State Key Laboratory of Fine Chemical, School of Chemical Engineering, Dalian University of Technology, Dalian, 116024, P. R. China. E-mail: zhaojzh@dlut.edu.cn; Web: http://finechem2.dlut.edu.cn/photochem

† Electronic supplementary information (ESI) available: Synthesis detail, molecular structure characterization data and more spectra. See DOI: 10.1039/c4tc02358g

(Scheme 1). The photoredox properties of the ligands and complexes were studied with cyclic voltammetry, whereas the photophysical properties of the complexes were studied with steady-state absorption, time-resolved absorption and emission spectroscopy. By introducing electron-withdrawing ligands (**L-2** and **L-3**), the photostability of the Pt(II) complexes were enhanced. At the same time, the redox properties and energy levels of the Pt(II) complexes were finely tuned and the C*N^N coordinated Pt(II) complexes (**Pt-4**) showed higher phosphorescence quantum yield than the C^N^N coordinated Pt(II) complexes (**Pt-3**), which is different from the results of Huo's work.[27] The redox and photophysical properties of the complexes were rationalized with DFT calculations. The Pt(II) complexes were used as triplet photosensitizers for triplet–triplet annihilation upconversion.

## Experimental section

### Analytical measurements

All the chemicals used in the syntheses were analytically pure and were used as received. Solvents were dried and distilled. 1-Bromopyrene (**1**), 2-ethylhexyl-4-bromo-1,8-naphthalimide (**2**), 1,6-dibromonaphthalene-1,2,6,7-tetracarboxylic dianhydrides (**3**), *N*,*N*′-di(2-ethylhexyl)-1,6-dibromonaphthalenetetracarboxylic diimides (**4**), 4-bromo-2,7-bis(2-ethylhexyl)-9-[(2-ethylhexyl) amino] (**5**), 2-bromo-6-(1-pyrazolyl)pyridine (**6**), 2-phenyl-6-(1*H*-pyrazol-1-yl)-pyridine (**m-1**), *N*,*N*-diphenyl-6-(1*H*-pyrazol-1-yl)-2-pyridinamine (**m-2**), **Pt-a** and **Pt-b** were synthesized according to previously reported methods (ESI† for synthesis and molecular structural characterization data).

**Complex Pt-3.** To a 25 mL dry, argon-flushed flask were charged complex **Pt-a** (45.0 mg, 0.10 mmol), **L-2** (43.6 mg, 0.13 mmol), CuI (3.5 mg, 0.018 mmol), i-$Pr_2NH$ (1 mL), and dichloromethane (10 mL). The mixture was stirred under Ar at room temperature for 24 h. The crude material was purified by flash chromatography (silica gel, dichloromethane) to give a yellow solid (35.1 mg, yield 47.0%). M.p.: 208.7–210.3 °C. $^1$H NMR (400 MHz, $CD_2Cl_2$) $\delta = 9.00$ (d, $J = 8.0$ Hz, 1H), 8.57 (d, $J = 3.5$ Hz, 1H), 8.49 (d, $J = 7.5$ Hz,1H), 8.12 (d, $J = 3.0$ Hz, 1H), 7.92 (d, $J = 1.5$ Hz, 1H), 7.86–7.80 (m, 3H), 7.78 (t, $J = 15.5$ Hz, 1H), 7.38 (t, $J = 18$ Hz, 2H), 7.21–7.16 (m, 2H),7.10 (t, $J = 14$ Hz, 1H), 6.68 (t, $J = 4.5$ Hz, 1H), 4.14–4.05 (m, 2H), 1.97–1.92 (m, $J = 6.8$ Hz, 1H), 1.41–1.29 (m, 8H) 0.95–0.88 (m, 6H). $^{13}$C NMR (100

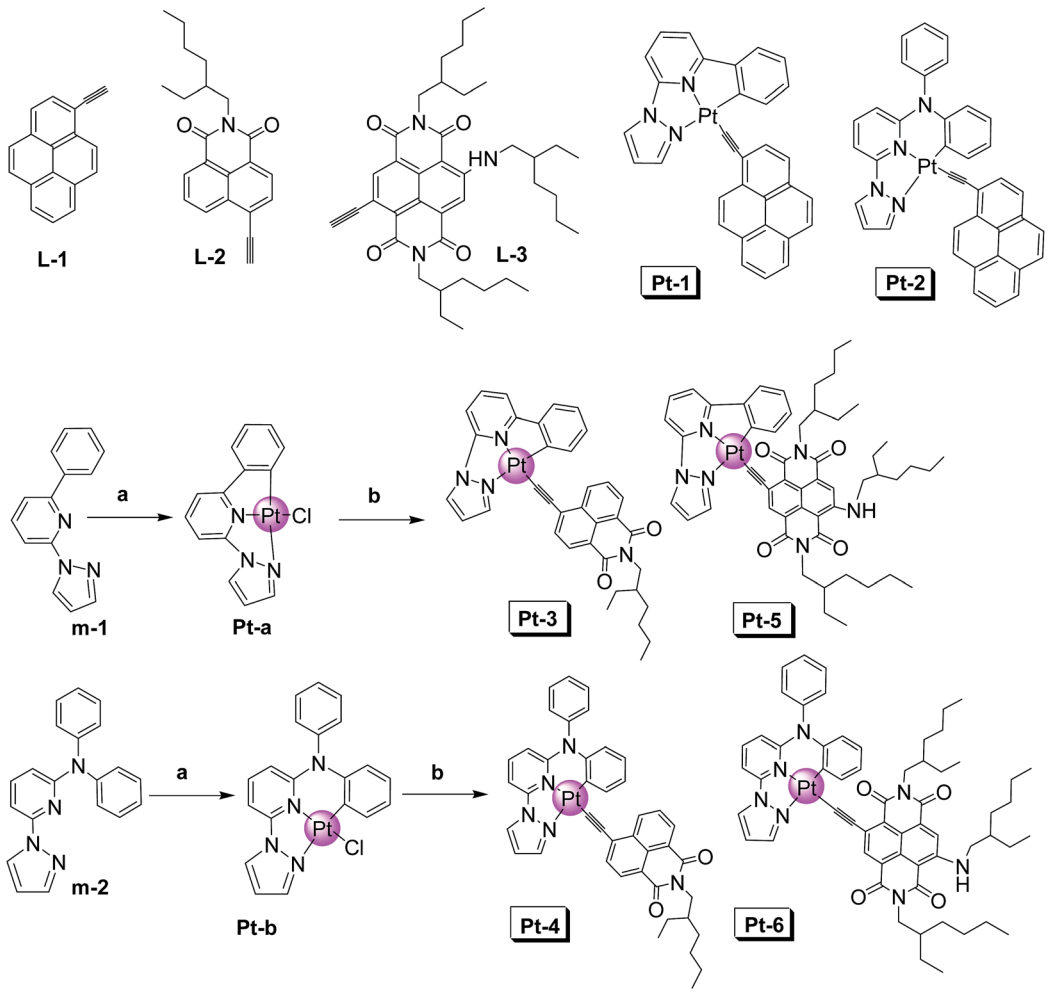


Scheme 1 Synthesis of the Pt(II) complexes and the structure of the ligands. (a) $K_2PtCl_4$ (1 equiv.), acetic acid, reflux, 22 h; (b) **L-2** or **L-3**, CuI, $CH_2Cl_2$, i-$Pr_2NH$, r.t., 24 h.

 

MHz, $CD_2Cl_2$) $\delta$ = 165.11, 164.85, 164.09, 148.25, 146.59, 144.68, 141.15, 140.21, 137.99, 134.25, 134.06, 133.02, 131.59, 131.30, 131.27, 130.55, 129.98, 128.91, 126.66, 125.34, 124.17, 123.37, 119.15, 115.89, 110.50, 106.64, 103.02, 44.23, 38.35, 31.16, 30.10, 29.16, 24.44, 23.52, 10.87. MALDI-HRMS: calcd ($[C_{36}H_{33}N_4O_2Pt + H]^+$): $m/z$ = 748.2251, found $m/z$ = 748.2239.

**Complex Pt-4.** This compound was prepared following the general procedure for complex **Pt-3**. The crude material was purified by flash chromatography (silica gel, dichloromethane) to give an orange solid (24.5 mg, yield 46.8%). M.p. >250 °C. $^1$H NMR (400 MHz, $CD_2Cl_2$) $\delta$ = 9.20 (d, $J$ = 24.3, 7.3 Hz, 1H), 8.62–8.52 (m, 3H), 8.41 (d, $J$ = 2.7 Hz, 1H), 8.35 (d, $J$ = 2.0 Hz, 1H), 7.98–7.89 (m, 1H), 7.82 (d, $J$ = 7.4 Hz, 1H), 7.74–7.57 (m, 6H), 7.22 (t, $J$ = 8.5 Hz, 1H), 6.90 (t, $J$ = 2.0 Hz, 1H), 6.83 (d, $J$ = 10.9, Hz, 1H), 6.74–6.68 (m, 1H), 6.62–6.50 (m, 2H), 4.16–4.05 (m, 2H), 2.01–1.87 (m, 1H), 1.44–0.85 (m, 14H). $^{13}$C NMR (100 MHz, $CD_2Cl_2$) $\delta$ = 167.98, 165.18, 164.90, 148.82, 147.97, 144.81, 144.11, 142.20, 140.59, 137.07, 134.35, 134.12, 133.21, 132.95, 131.88, 131.31, 131.27, 130.79, 130.02, 129.49, 129.15, 128.99, 128.73, 126.79, 124.47, 123.43, 122.42, 119.37, 119.31, 119.14, 115.42, 114.78, 110.77, 100.40, 98.58, 44.27, 38.41, 31.23, 30.81, 29.20, 24.52, 23.52, 10.9. MALDI-HRMS: calcd ($[C_{42}H_{38}N_5O_2Pt]^+$): $m/z$ = 839.2637, found $m/z$ = 839.2642.

**Complex Pt-5.** This compound was prepared following the general procedure for complex **Pt-3**. The crude material was purified by flash chromatography (silica gel, dichloromethane) to give a red solid (15.9 mg, yield 32.5%). M.p.: 189.5–191.7 °C. $^1$H NMR (400 MHz, $CDCl_3$) $\delta$ = 10.02 (t, $J$ = 4.4 Hz, 1H), 8.93–8.82 (m, 2H), 8.42–8.21 (m, 3H), 8.12 (t, $J$ = 8.1 Hz, 1H), 7.86 (d, $J$ = 8.0 Hz, 1H), 7.71 (d, $J$ = 7.3 Hz, 1H), 7.58 (d, $J$ = 7.0 Hz, 1H), 7.49 (t, $J$ = 7.2 Hz, 1H), 7.12 (t, $J$ = 7.6 Hz, 1H), 6.87 (t, $J$ = 6.8 Hz,1H), 4.34–4.03 (m, 4H), 3.51 (t, $J$ = 5.6 Hz, 2H), 2.00 (d, $J$ = 10.3 Hz, 2H), 1.81 (t, $J$ = 12.0 Hz, 1H),1.56–1.25 (m, 28H),1.02–0.88 (m, 14H). MALDI-HRMS: calcd ($[C_{54}H_{65}N_5O_4Pt + H]^+$): $m/z$ = 1056.4751, found $m/z$ = 1056.4736.

**Complex Pt-6.** The compound was prepared following the general procedure for complex **Pt-3**. The crude material was purified by column chromatography (silica gel, dichloromethane) to give a red solid (13.5 mg, yield 37.8%). M.p.: 167.4–169.2 °C. $^1$H NMR (400 MHz, $CDCl_3$) $\delta$ = 10.05 (t, $J$ = 4.7 Hz, 1H), 9.43 (d, $J$ = 1.8 Hz, 1H), 8.99–8.85 (m, 2H), 8.35–8.24 (m, 2H), 7.76–7.51 (m, 6H), 7.07 (d, $J$ = 9.2 Hz, 2H), 6.90–6.82 (m, 1H), 6.71 (t, $J$ = 8.4 Hz, 1H), 6.48 (d, $J$ = 8.8 Hz, 2H), 4.30–4.10 (m, 4H), 3.52 (t, $J$ = 5.6 Hz, 2H), 2.09–1.90 (m, 2H), 1.85–1.73 (m, 1H), 1.46–1.25 (m, 28H),1.03–0.87 (m, 14H). MALDI-HRMS: calcd ($[C_{60}H_{70}N_7O_4Pt + H]^+$): $m/z$ = 1147.5137, found $m/z$ = 1147.5057.

**Nanosecond time-resolved transient difference absorption spectroscopy.** Nanosecond time-resolved transient difference absorption spectra were recorded using a LP 920 laser flash photolysis spectrometer (Edinburgh Instruments, Livingston, UK). The samples were purged with $N_2$ or argon for 30 min before measurement. The samples were excited with a nanosecond pulsed laser (Vibrant 355II, wavelength tunable in the range of 410–2400 nm), and the transient signals were recorded using a Tektronix TDS 3012B oscilloscope.

**TTA upconversion.** Diode-pumped solid state laser was used for upconversions (445 nm). The laser power was measured with a phototube. The mixed solution of the Pt(II) complex (triplet photosensitizer) and DPA (triplet acceptor) was degassed for at least 15 min with $N_2$ or argon before measurement. The spectra were recorded using an adapted RF5301PC spectrofluorometer (Shimadzu, Japan).

**The delayed fluorescence of the upconversion ($\tau_{DF}$).** The delayed fluorescence ($\tau_{DF}$) was measured with an Opolette™ 355II + UV nanosecond pulsed laser (typical pulse length: 7 ns, pulse repetition: 20 Hz, peak OPO energy: 4 mJ, wavelength tunable in the range of 210–355 nm and 410–2200 nm, OPOTEK, USA), which was synchronized to a FLS 920 spectrofluorometer (Edinburgh, UK). The decay kinetics of the upconverted fluorescence (delayed fluorescence) was monitored with a FLS920 spectrofluorometer. The prompt fluorescence lifetime of the triplet acceptor perylene was measured with an EPL picosecond pulsed laser (405 nm), which was synchronized to the FLS 920 spectrofluorometer.

**Theoretical calculations.** DFT calculations with a B3LYP/6-31G/LANL2DZ basis set were used for the optimization of both the ground-state and triplet states. The energy levels of the $T_1$ states (energy gap between $S_0$ and $T_1$) were calculated with time-dependent DFT (TDDFT) calculations on the basis of optimized triplet state geometries. All the calculations were carried out with Gaussian 09W.[29]

# Results and discussion

### Design and synthesis of molecules

The C^N^N ligand and the C*N^N ligand with different redox potential properties were selected to form Pt(II) coordination center **Pt-a** and **Pt-b**. Recently, it was reported that the coordination geometry of **Pt-a** is a perfect square planar structure,[27] thus photoluminescence efficiency based on **Pt-a** is high. However, photoredox properties (driving forces for charge transfer) and their energy levels of emission and absorption (driving forces for energy transfer) also play important roles in the photoluminescence efficiency. Introducing different arylacetylide ligands would have substantial influence on the properties mentioned above, further affecting the photoluminescence efficiency. To study the synergetic effect of the arylacetylide ligands and C^N^N/C*N^N Pt coordination center on the photoredox and photophysical properties of the complexes, Py was selected as the ligand. It was reported that complexes with pyrenyl acetylide ligands gave long-lived triplet excited states.[28,30] However, the corresponding Pt(II) complexes (**Pt-1** and **Pt-2**) were not stable. Therefore, NI and NDI acetylide ligands, with strong electron withdrawing ability, were used as ligands to enhance the stability of the Pt(II) complexes. Herein these arylacetylide ligands were used for the investigation of the effect of C^N^N/C*N^N ligands and acetylides on the photoredox and photophysical properties of the Pt(II) complexes. The synthesis procedure is based on routine methods. All the complexes were obtained with moderate to satisfactory yields.

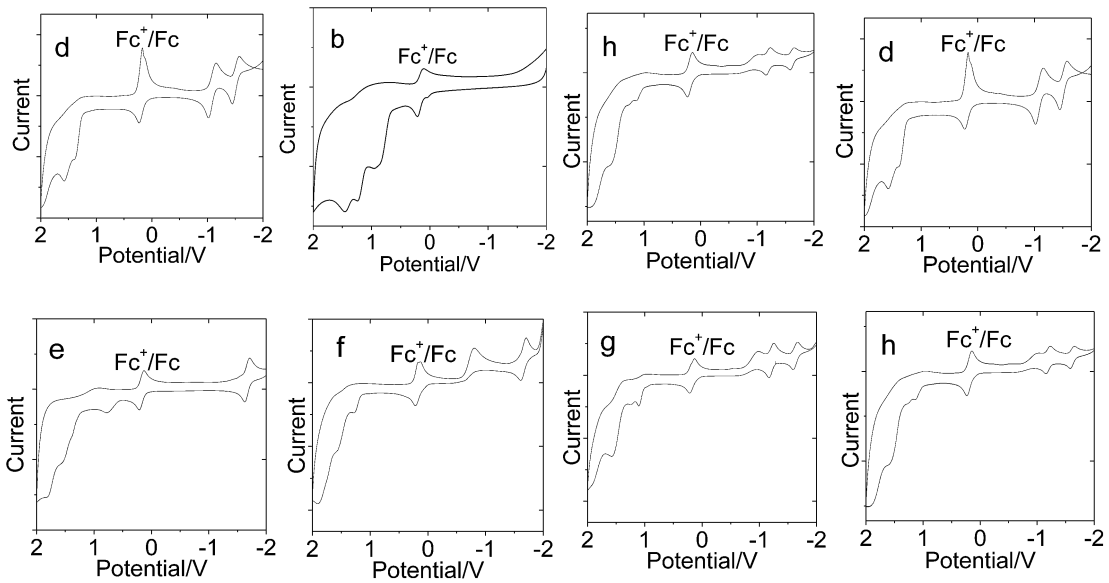


Fig. 1 Cyclic voltammogram of (a) **Pt-a**, (b) **Pt-b**, (c) **L-2**, (d) **L-3**, (e) **Pt-3**, (f) **Pt-4**, (g) **Pt-5** and (h) **Pt-6**. In deaerated $CH_2Cl_2$ solutions containing 1.0 mM photosensitizers with ferrocene in 0.10 M $Bu_4NPF_6$ as supporting electrode, $Ag/AgNO_3$ as reference electrode and scan rate: 50 mV $s^{-1}$. Ferrocene (Fc) was used as internal reference.

### Electrochemical data of the complexes

The electrochemical properties of the ligands and complexes were studied with cyclic voltammetry (Fig. 1). For complex **Pt-a**, oxidation waves at +0.6 V and +1.01 V were observed, which could be assigned to the C^N^N Pt(II) coordination center. No reduction wave was found. These results indicate the possibility of charge transfer from the C^N^N Pt(II) coordination center to the arylacetylide ligand (MLCT). For **Pt-b**, a few oxidation waves at +0.91 V, +1.17 V and +1.39 V were observed, wherein the oxidation waves at +1.17 V could be assigned to the structure of *N*,*N*-diphenylpyridineamine in the C*N^N Pt(II) coordination center.[31] The other two waves at +0.91 V and +1.39 V could be assigned to the C*N^N Pt(II) coordination center. The use of an aniline linker breaks the $\pi$ conjugation of the C*N^N Pt(II) coordination center, resulting in an evident positive shift (above 0.30 V). For the ethynyl NI ligand (**L-2**), a reduction wave at −1.45 V was observed, indicating that **L-2** is a good electron acceptor. For the NDI acetylide ligand (**L-3**), two reversible reduction waves at −1.02 V and −1.45 V were observed. For **Pt-3** with NI acetylide ligands (electron withdrawing substituents), the reduction wave at −1.62 V and the oxidation wave at 1.51 V were observed, which can be assigned to the NI acetylide ligand. The oxidation wave at +0.77 V was observed and can be assigned to the C^N^N Pt(II) coordination center. Compared with **Pt-a**, the oxidation potential of **Pt-3** shows a 0.17 V positive shift, indicating perturbation of the electronic structure of the NI ligand. At the same time, the more positive oxidation potential enhances the stability of Pt(II) complexes.[32] On the other hand, no reversible reduction wave was observed, which is different from **Pt-a**, indicating that the coordination of NI acetylide ligand to the Pt(II) center imposes a substantial influence on the electronic structure of the C^N^N Pt(II) coordination center. For **Pt-4**, the onset oxidation wave was observed at +1.27 V. Compared with **Pt-b**, **Pt-4** shows a 0.36 V positive shift, indicating that the electronic structure of the NI ligand is substantially altered upon coordination to the Pt(II) atom. Thus, the effects of the C^N^N or the C*N^N ligand are different. Similar results were also observed for **Pt-5** and **Pt-6**. The electrochemical data for the complexes and the ligands are listed in Table 1. Complexes **Pt-1** and **Pt-2** with Py ligands are unstable, thus their CV data were not collected.

In order to further investigate the charge transfer process (MLCT), the thermodynamic driving forces for the charge transfer process ($\Delta G^\circ$, free energy change of the potential charge transfer) were calculated based on the redox potential values, by employing the Rehm–Weller Equation (eqn (1)).[33]

Table 1 Electrochemical data for **Pt-a**, **Pt-b**, **L-2**, **L-3**, **Pt-3**, **Pt-4**, **Pt-5** and **Pt-6**

| | Oxidation[a] (V) | | | Reduction[a] (V) | | |
|---|---|---|---|---|---|---|
| Compd | I | II | III | I | II | $\Delta G^{\circ c}$ (eV) |
| **Pt-a** | +0.60 | +1.01 | —[b] | —[b] | —[b] | —[b] |
| **Pt-b** | +0.91 | +1.17 | +1.39 | —[b] | —[b] | —[b] |
| **L-2** | +1.53 | —[b] | —[b] | −1.45 | —[b] | —[b] |
| **L-3** | +1.57 | —[b] | —[b] | −1.02 | −1.45 | —[b] |
| **Pt-3** | +0.77 | +1.51 | —[b] | −1.62 | —[b] | −0.73 |
| **Pt-4** | +1.27 | +1.55 | —[b] | −1.61 | —[b] | +0.00 |
| **Pt-5** | +1.10 | +1.58 | —[b] | −1.16 | −1.59 | +0.04 |
| **Pt-6** | +1.12 | +1.57 | —[b] | −1.15 | −1.59 | −0.05 |

[a] Recorded with $[Bu_4N][PF_6]$ as the electrolyte in $CH_2Cl_2$ (0.1 M) at ambient temperature with a scan rate of 50 mV $s^{-1}$. Potentials are expressed as the half-wave potentials ($E_{1/2}$) in volts *vs.* $Ag/AgNO_3$ using ferrocene as an internal reference. [b] Not determined. [c] Free energy changes of the potential PET effect with Rehm–Weller equation.

 

$$\Delta G^{\circ} = E_{ox} - E_{red} - E_{0,0} - C \quad (1)$$

where $\Delta G^{\circ}$ is the free energy change of the potential charge transfer. $E_{ox}$ is the oxidation potential of the electron donor (Pt coordination center), $E_{red}$ is the reduction potential of the electron acceptor (acetylide ligand), $E_{0,0}$ is the excitation energy, which is calculated based on the wavelength of the maximum absorption in the visible region and $C$ could be regarded as a constant, which is related to the solvents. These measurements were obtained in the same solvent, so $C$ could be ignored [eqn (1)].

**Pt-3** shows a more negative $\Delta G^{\circ}$ value (−0.73 eV) than the other complexes, indicating that its charge transfer process is enhanced (Table 1 and ESI†). **Pt-3** has the lower phosphorescence quantum yield (*vide infra*). For **Pt-4**, the more positive onset oxidation potential (1.27 V) contributes to the increase of $\Delta G^{\circ}$ (0.00 eV), as **Pt-4** shows significantly higher $\Delta G^{\circ}$ than that of **Pt-3**, which means considerably weaker ability to undergo charge transfer process thermodynamically. The phosphorescence quantum yield of **Pt-4** is enhanced ($\Phi_P = 0.14$). Although the $\Delta G^{\circ}$ of **Pt-5** (0.04 eV) is higher than that of **Pt-4** (0.00 eV), the phosphorescence quantum yield of **Pt-5** is still lower than that of **Pt-4** ($\Phi_P = 0.14$). Therefore, energy levels also need to be considered for the design of Pt(II) complexes (*vide infra*).

## Steady state UV-Vis absorption and luminescence emission spectroscopy

The absorption spectra of **Pt-a** and **Pt-b** are shown in Fig. 2a. The spectra show strong absorptions in the high-energy region and weaker absorptions in the low-energy region. The high-energy absorptions can be assigned as ligand based π–π* transitions, whereas the low energy absorptions can be assigned as charge transfer bands.[27] The $S_0 \rightarrow {}^1$MLCT absorption bands in parent complexes **Pt-a** and **Pt-b** were observed at 390 nm and 419 nm, respectively. The UV-Vis absorption spectra of the ligands were studied (see ESI†). **L-1** gives absorption in the UV region. The molar absorption coefficient ($\varepsilon$) is $4.92 \times 10^4$ $M^{-1}$ $cm^{-1}$ at 360 nm. The intense structured absorption of the pyrenylacetylide was reduced in the complexes **Pt-1** and **Pt-2** (Fig. 2b). Moreover, the absorption intensity was reduced as compared with that of the free ligands. These results indicate that the π-conjugation framework of **L-1** is substantially perturbed in the complexes **Pt-1** and **Pt-2**. This is reasonable since the Pt(II) atom is linked to the pyrenyl moiety by the C≡C triple bond.[34] Similar results were observed for **Pt-3** and **Pt-4** (Fig. 2c). Moreover, the maximum absorption wavelength of the complexes **Pt-3** and **Pt-4** are considerably red-shifted as compared with that of ligand **L-2**. Based on the DFT/TDDFT calculations, the intense absorption of **Pt-3** at 397 nm could be attributed to the mixed $^1$MLCT and $^1$IL excited states (see ESI†). These results are in accordance with photoredox properties ($\Delta G^{\circ} = -0.73$ eV). The absorption of **Pt-4** at 431 nm could be attributed to the energy level of the $^1$IL excited state. The photoredox properties ($\Delta G^{\circ} =$ 0.00 eV) and DFT/TDDFT calculations (Table 3) also confirmed that **Pt-4** shows less MLCT character than **Pt-3**. **Pt-5** and **Pt-6** show similar absorption wavelength as compared with the ligand **L-3** (Fig. 2d). The absorptions of **Pt-5** and **Pt-6** at around

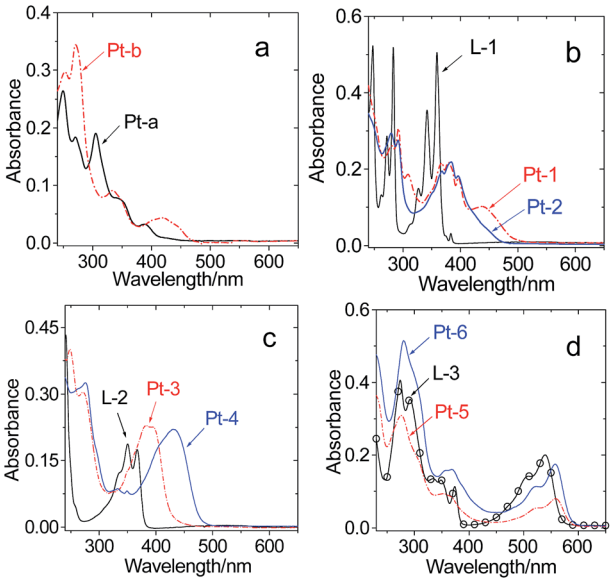


Fig. 2 UV-Vis absorption of (a) **Pt-a** and **Pt-b**; (b) **L-1**, **Pt-1** and **Pt-2**; (c) **L-2**, **Pt-3** and **Pt-4**; (d) **L-3**, **Pt-5** and **Pt-6**. $c = 1.0 \times 10^{-5}$ M in dichloromethane (DCM), 20 °C.

559 nm could be attributed to their $^1$IL excited states. These results are also confirmed by the DFT/TDDFT calculations (see ESI†).

The UV-Vis absorption spectra of the ligands and the complexes in different solvents were studied. The low energy absorptions of **Pt-3** showed a slight solvent dependence and shifted to higher energy by up to 23 nm as the solvents switched from toluene to MeOH, indicating that these low energy transitions possess, to some extent, charge transfer character. No significant changes were observed for **Pt-4**, **Pt-5** and **Pt-6** (ESI†), indicating that this absorption could be attributed to the $^1$IL excited state.

The photoluminescences of the complexes were studied (Fig. 3a and b). For complexes **Pt-1** and **Pt-2**, strong emission at 660 nm was observed, which is highly sensitive to $O_2$. The emission can be completely quenched in aerated solution. Thus the emission is due to emissive triplet excited states. This postulation is in agreement with the previous observation of phosphorescence with pyrenylacetylide Pt(II) complexes.[15]

Interestingly, the emission properties of **Pt-3** and **Pt-4** were drastically different. For **Pt-3** (Fig. 3c), the major emission band is centered at 434 nm, for which the emission intensity is independent of the atmosphere (air or $O_2$), thus the emission band at 434 nm can be assigned to fluorescence. Moreover, a minor emission band at 629 nm was observed, which can be quenched by $O_2$. Thus the emission band can be assigned to phosphorescence. The emission band at 434 nm is not due to any impurity of free ligand in the complex, because the emission wavelength is considerably longer than that of the ligand **L-2**. The different emission properties of **Pt-3** and **Pt-4** can be rationalized by the different influence of the ligands, demonstrated by the cyclic voltametry study as well as the UV-Vis absorption spectra of the complexes **Pt-3**

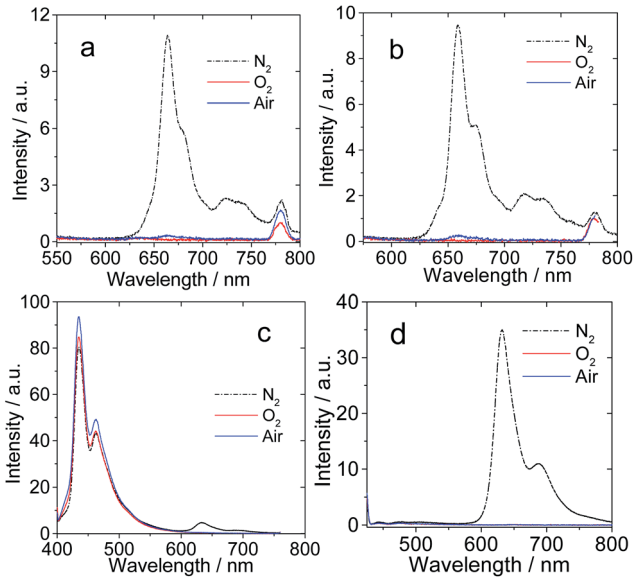


Fig. 3 The emission spectra of the Pt(II) complexes under different atmospheres. (a) **Pt-1** ($\lambda_{ex}$ = 390 nm); (b) **Pt-2** ($\lambda_{ex}$ = 390 nm); (c) **Pt-3** ($\lambda_{ex}$ = 390 nm); (d) **Pt-4** ($\lambda_{ex}$ = 420 nm). $c = 1.0 \times 10^{-5}$ M in toluene, 20 °C.

and **Pt-4**. The $\Delta G^{\circ}$ value of **Pt-4** is 0.00 eV, which shows a good balance of the energy transfer and charge transfer. The phosphorescence emission of **Pt-4** is assigned to $^3$IL (*vide infra*). The phosphorescence quantum yield is up to 0.14, which is higher than for other complexes. To study the triplet state yields of the complexes, the photosensitization of singlet oxygen ($^1O_2$) with the complexes upon photoexcitation was studied and the $^1O_2$ quantum yields ($\Phi_\Delta$) were determined (Table 2). The $^1O_2$ quantum yields ($\Phi_\Delta$) with **Pt-4** as triplet photosensitizer was determined as 0.65, indicating efficient intersystem crossing (ISC).

The $\Delta G^{\circ}$ value of the electron transfer in **Pt-3** was calculated as −0.7 eV. The singlet oxygen quantum yield of **Pt-3** is 0.57, indicating efficient intersystem crossing.

The emission of **Pt-5** and **Pt-6** are centered at 570 nm, which are not dependent on the atmosphere of the solution, thus the emission bands can be assigned to fluorescence (ESI†). Similar to **Pt-1**, the emission bands of **Pt-5** and **Pt-6** are different from that of the free ligand **L-3**, thus the emission band of **Pt-5** and **Pt-6** are not due to the un-coordinated free ligand. At the same time, the energy level of the $^1$IL state (2.22 eV) is considerably lower than that of the $^1$MLCT state (3.02 eV); therefore, the $^1$IL → $^1$MLCT process is inhibited. These reasons cause the non-phosphorescence. The singlet oxygen quantum yield of **Pt-5** ($\Phi_\Delta$ = 0.07) also infers the poor triplet state yield, which confirms the results mentioned above and not the limit of detection range of the spectrophotometer.

The $\Delta G^{\circ}$ value of **Pt-6** is −0.05 eV. Due to the weak charge transfer impetus (low $\Delta G^{\circ}$ value), the charge transfer process from the Pt(II) coordination center to NDI ligand is inefficient. **Pt-6** shows no phosphorescence, and the singlet oxygen quantum yield of **Pt-6** is 0.09.

To clarify the electronic feature of the emissive triplet excited state of the complexes, *i.e.* as $^3$MLCT state or $^3$IL state, the emission spectra of **Pt-4** at 77 K was compared with that at RT (Fig. 4). The emission band at 77 K is slightly blue-shifted as compared with that at RT. The thermally induced Stokes shift is 245 cm$^{-1}$. The emission band at 77 K is more structured than that at RT. Thus the emissive triplet excited state of **Pt-4** can be assigned as the $^3$IL state, for a charge transfer state, such as $^3$MLCT state, a more significant thermally induced Stokes shift will be observed.

## Nanosecond time-resolved transient difference absorption spectroscopy

To study the triplet excited states of the complexes, nanosecond time-resolved transient difference absorption spectra of the

Table 2 Photophysical parameters of **Pt-1**–**Pt-6**, **L-1**, **L-2** and **L-3**

| | $\lambda_{abs}$[a] | $\varepsilon$[b] | $\lambda_{em}$[c] | $\Phi_F$ | $\Phi_P$ | $\tau_F$[g] (ns) | $\tau_P$[h] (μs) | | $\tau_T$[i]/μs | $\Phi_\Delta$[j] |
|---|---|---|---|---|---|---|---|---|---|---|
| | | | | | | 298 K | 298 K | 77 K | | |
| **Pt-1** | 400 | 1.61 | 663 | —[k] | 0.9[f]% | —[k] | —[k] | | —[k] | —[k] |
| **Pt-2** | 398 | 2.06 | 659 | —[k] | 3.6[f]% | —[k] | —[k] | | —[k] | —[k] |
| **Pt-3** | 397 | 2.48 | 434\629 | 5.7[f]% | 0.6[f]% | 4.50 | 30.6<br>—[k] | | —[k] | 0.57 |
| **Pt-4** | 431 | 2.26 | 631 | —[k] | 14.4[f]% | —[k] | 137.0<br>250.9 | | 90.1 | 0.65 |
| **Pt-5** | 559 | 0.88 | 564 | 3.5[d]% | —[k] | 9.69 | —[k] | | —[k] | 0.07 |
| **Pt-6** | 558 | 1.69 | 582 | 0.6[d]% | —[k] | 9.37 | —[k] | | —[k] | 0.09 |
| **L-1** | 360 | 4.92 | 384\404 | 8.9[e]% | —[k] | 3.32 | —[k] | | —[k] | —[k] |
| **L-2** | 350 | 1.74 | 400 | 7.6[e]% | —[k] | 2.21 | —[k] | | —[k] | —[k] |
| **L-3** | 536 | 1.98 | 561 | 16.9[e]% | —[k] | 11.43 | —[k] | | —[k] | —[k] |

[a] In toluene ($1.0 \times 10^{-5}$ mol dm$^{-3}$). [b] Molar extinction coefficient at the absorption maxima. $\varepsilon$: $10^4$ cm$^{-1}$ mol$^{-1}$ dm$^3$. [c] In toluene. [d] In toluene, with 2,6-diiodo-Bodipy ($\Phi$ = 0.027 in acetonitrile) as the standards. [e] In toluene, with quinine sulfate ($\Phi$ = 0.546 in 0.5 M $H_2SO_4$) as the standards. [f] In toluene, with $[Ru(dmb)_3(PF_6)_2]$ ($\Phi$ = 0.073 in acetonitrile) as the standards. [g] Luminescence lifetime, **Pt-3** ($\lambda_{ex}$ = 443 nm), **Pt-5** and **Pt-6** ($\lambda_{ex}$ = 473 nm) at RT. [h] Phosphorescence lifetime, **Pt-3** ($\lambda_{ex}$ = 397 nm) and **Pt-4** ($\lambda_{ex}$ = 431 nm) at RT. [i] Triplet state lifetimes, measured by nanosecond transient difference absorption spectroscopy. [j] Quantum yield of singlet oxygen ($^1O_2$), for **Pt-3** and **Pt-4**, $[Ru(bpy)_3(PF_6)_2]$ was used as standard ($\Phi_\Delta$ = 0.57 in acetonitrile), for **Pt-5** and **Pt-6**, 2,6-diiodo-Bodipy was used as standard ($\Phi_\Delta$ = 0.79 in $CH_2Cl_2$), $c = 1.0 \times 10^{-5}$ M in acetonitrile. [k] Not applicable.

 

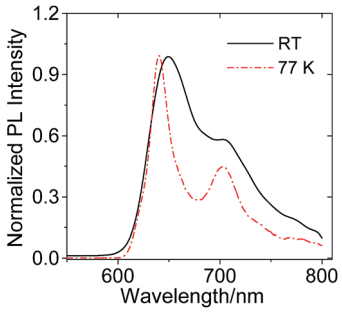


Fig. 4 Photoluminescence spectra of **Pt-4** at room temperature (RT) and 77 K ($\lambda_{ex}$ = 425 nm). $c = 2.0 \times 10^{-5}$ M in mixed solvent $C_2H_5OH$–$CH_3OH$ (4 : 1, v/v).

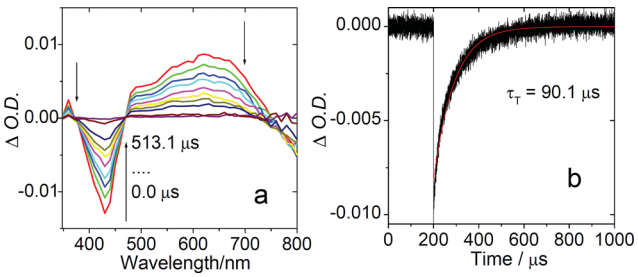


Fig. 5 Nanosecond time-resolved transient difference absorption spectra of (a) **Pt-4** after pulsed excitation ($\lambda_{ex}$ = 430 nm). (b) Decay traces of **Pt-4** at 450 nm. $c = 1.0 \times 10^{-5}$ M in deaerated toluene, 25 °C.

complexes were investigated (Fig. 5).[9] For **Pt-4**, a bleaching band at 430 nm was observed upon excitation with 430 nm nanosecond pulsed laser. Moreover, a strong transient absorption band in the region of 470–740 nm was observed, which can be assigned to the absorption of the $T_1$ state ($T_1 \rightarrow T_n$ transitions).[25] The lifetime was determined as 90.1 μs (at $c = 1.0 \times 10^{-5}$ M). The triplet state lifetime is long, thus triplet–triplet annihilation of **Pt-4** has to be considered, with which the lifetime can be reduced at high concentration. Therefore, the triplet state lifetime of the complex was measured at lower concentration; the intrinsic triplet state lifetime of **Pt-4** was extrapolated as 126.7 μs (in infinite diluted solution, ESI†).

No transient spectra can be observed for **Pt-5** and **Pt-6** under photoexcitation at 555 nm and 560 nm, respectively, which may be due to the poor triplet quantum yield. Because **Pt-1** and **Pt-2** are not stable, no transient absorption spectra were recorded for these two complexes.

## DFT calculations

The ground state geometries of the complexes were optimized using DFT methods. For **Pt-4** (Fig. 6 and Table 3), the UV-Vis absorption was calculated based on the optimized ground state geometry. The absorption band in the visible region was predicted to be at 459 nm, which is close to the experimental result of 431 nm (Fig. 3b). It is known that DFT methods usually underestimate the excitation energy for charge transfer transitions. The electronic components of the $S_0 \rightarrow S_1$ transition are

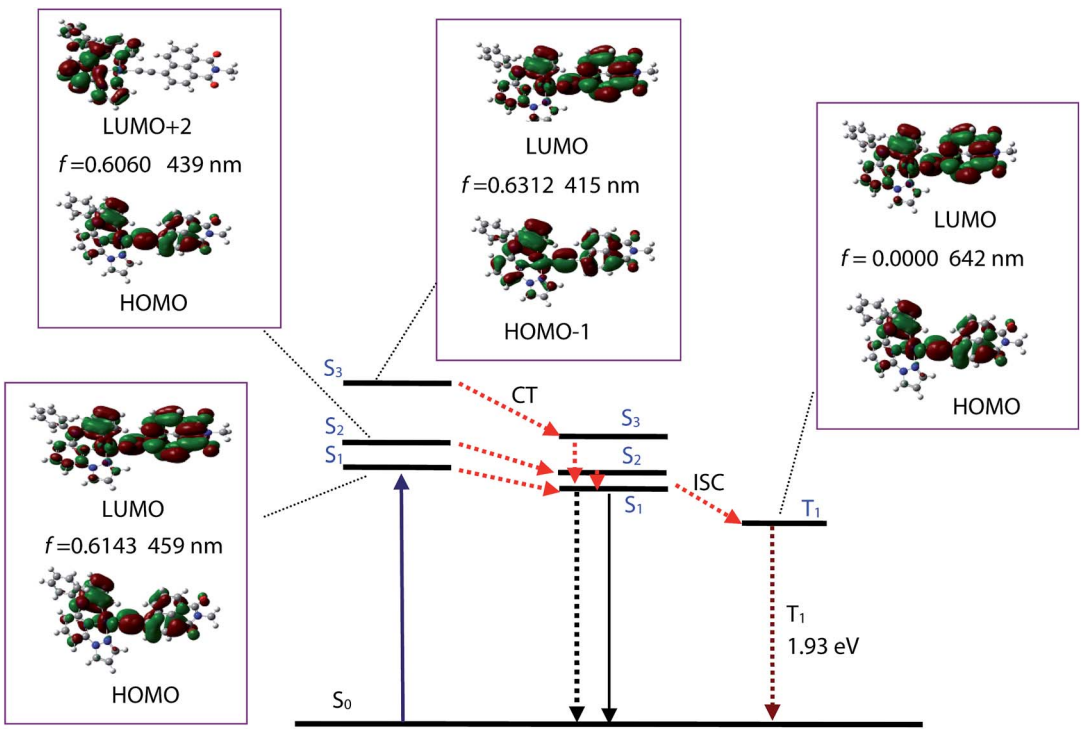


Fig. 6 Selected frontier molecular orbitals involved in the excitation and the singlet/triplet excited states of **Pt-4**. CT stands for conformation transformation. The left column is UV-Vis absorption (based on the ground state geometry) and the right column is the triplet excited state (based on the ground state geometry). For clarity, only the selected excited states were presented. The calculations are at the B3LYP/6-31G/LANL2DZ level using Gaussian 09W.

Table 3 Selected electronic excitation energies (eV) and corresponding oscillator strengths (*f*), main configurations and CI coefficients of the low-lying electronically excited states of **Pt-4**. Based on the optimized ground state geometries, the calculations are at the B3LYP/6-31G/LANL2DZ level using Gaussian 09W

| | | TDDFT//B3LYP/6-31G | | | | |
|---|---|---|---|---|---|---|
| **Pt-4** | Electronic transition | Energy[a] (eV) | *f*[b] | Composition[c] | CI[d] | Character |
| Singlet | $S_0 \rightarrow S_1$ | 2.70 eV/459 nm | 0.3550 | H → L | 0.6143 | ILCT |
| | | | | H → L + 1 | 0.3102 | ILCT |
| | $S_0 \rightarrow S_2$ | 2.82 eV/439 nm | 0.0896 | H − 1 → L + 1 | 0.1364 | MLCT, ILCT |
| | | | | H → L | 0.3016 | ILCT |
| | | | | H → L + 2 | 0.6060 | ILCT |
| | $S_0 \rightarrow S_3$ | 2.99 eV/415 nm | 0.2449 | H − 1 → L | 0.6312 | MLCT,ILCT |
| | $S_0 \rightarrow S_4$ | 3.10 eV/401 nm | 0.0961 | H − 1 → L + 1 | 0.6351 | MLCT,ILCT |
| Triplet | $S_0 \rightarrow T_1$ | 1.93 eV/642 nm | 0.0000 | H → L | 0.5094 | ILCT |
| | | | | H − 1 → L | 0.4382 | MLCT,ILCT |
| | $S_0 \rightarrow T_2$ | 2.57 eV/483 nm | 0.0000 | H → L + 1 | 0.5226 | ILCT |
| | $S_0 \rightarrow T_3$ | 2.77 eV/447 nm | 0.0000 | H − 1 → L | 0.4069 | MLCT,ILCT |
| | | | | H → L | 0.4102 | ILCT |

[a] Only selected excited states were considered. The numbers in parentheses are the excitation energy in wavelength. [b] Oscillator strength. [c] H stands for HOMO and L stands for LUMO. Only the main configurations are presented. [d] Coefficient of the wave function for each excitation. The CI coefficients are in absolute value.

H → L, which can be assigned as the IL and MLCT mixed transition with IL as the major component. The singlet–triplet state energy gaps were also calculated. The energy level of the $T_1$ state was estimated to be 1.93 eV (642 nm). H → L is involved in the $T_1$ state, thus the $T_1$ state can be assigned as the $^3$IL state, which is in agreement with the spin density analysis and the long lived triplet excited state observed for **Pt-4**. The geometries of **Pt-3**, **Pt-5** and **Pt-6** were also optimized. The calculated absorption is close to the experimental observations (ESI†).

To assign the triplet states of the complexes, the spin density surfaces were calculated by DFT methods.[35–37] For **Pt-a** and **Pt-b**, the spin density surfaces are located in the tridentate ligand and Pt(II) coordination centers, which could be assigned as $^3$MLCT states (Fig. 7). The triplet excited states of the Pt(II) complexes are localized on the acetylide ligands. This is in agreement with the long-lived triplet excited states of the complexes.

### Triplet–triplet annihilation upconversion

Triplet–triplet annihilation (TTA) upconversion has attracted considerable attention due to the advantages of low excitation light power threshold, high upconversion quantum yields, and tunable excitation/emission wavelength.[38,39] A triplet photosensitizer is crucial for TTA upconversion.[40] Thus, it is important to develop new triplet photosensitizers for TTA upconversion. To the best of our knowledge, very few tridentate cyclometalated Pt(II) acetylide complexes have been used as triplet photosensitizers for TTA upconversion.[28,35] Herein the Pt(II) complexes were used for TTA upconversion. **Pt-4** shows strong absorption of visible light and long-lived triplet excited state. TTA upconversion with **Pt-4** as the triplet photosensitizer was studied (Fig. 8). Upon 445 nm laser excitation, a phosphorescence band at 634 nm was observed. A triplet acceptor is an essential component for TTA upconversion.[8,9] One of the prerequisites for a useful triplet photosensitizer is that the energy level of the $T_1$ state of a triplet acceptor must be lower than the energy level of the $T_1$ state of the photosensitizer.

Based on the $T_1$ state energy level of **Pt-4** ($\lambda_{em}$ = 631 nm, 1.97 eV), 9,10-diphenylanthracene (DPA) was selected as the triplet acceptor ($T_1$ state energy level is 1.77 eV). In the presence of the triplet acceptor, strong emission in the region of 400–500 nm was observed. This is due to the upconverted fluorescence emission of DPA. Excitation of DPA alone at 445 nm did not give any emission in the region of 400–500 nm, thus the TTA upconversion with **Pt-4**/DPA is verified. The triplet–triplet annihilation upconversion and upconversion quantum yield was determined as 29.7%, which is very high for TTA upconversion.[8,9]

To confirm the TTA upconversion, the luminescence lifetime of the TTA upconversion emission was determined (Fig. 9). The

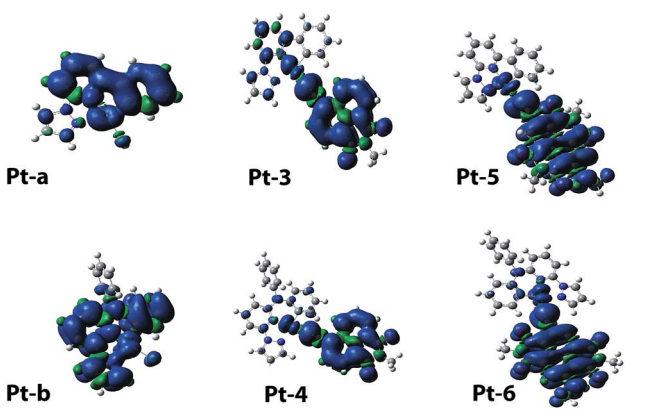


Fig. 7 Spin density of the complexes **Pt-a**, **Pt-b**, **Pt-3**–**Pt-6** at the optimized triplet state geometries. Toluene was used as the solvent in the calculations. Calculation was performed at B3LYP/6-31G/LANL2DZ level with Gaussian 09W.

 

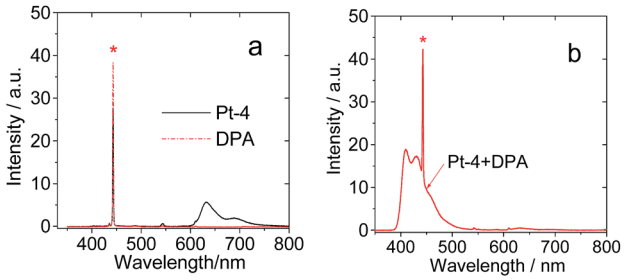


Fig. 8 Emission and upconversion of the complexes with 445 nm (5.2 mW) laser excitation. (a) Emission of the complexes alone. (b) The upconverted DPA fluorescence and the residual fluorescence and phosphorescence of **Pt-4**. The asterisks in (a) and (b) indicate the scattered 445 nm excitation laser (5.2 mW). $c$[DPA] = 4.0 × $10^{-5}$ M; $c$ [sensitizers] = 1.0 × $10^{-5}$ M in deaerated toluene, 25 °C.

luminescence lifetime was determined as 324.9 μs. On the contrary, the luminescence lifetime of the prompted fluorescence of DPA was determined as 7.3 ns. Thus the TTA upconversion was proved.

The images of the luminescence of the sensitizers alone and the upconversion are shown in Fig. 10. The upconversion with **Pt-4** as the triplet photosensitizer is clearly visible to the unaided eyes. **Pt-4** alone gives red emission, whereas the mixed solution of **Pt-4** and DPA shows a purple emission. However, the emission wavelength of the **Pt-3** solution does not change in the presence of DPA, indicating the lack of TTA upconversion for **Pt-3**, which is due to its poor absorption ability at 445 nm. For **Pt-5** and **Pt-6**, no upconverted blue emission was observed, which is attributed to the low quantum yield of the triplet excited state. The changes in the emission color of the triplet photosensitizers with and without the triplet acceptor DPA were quantified with the CIE coordinates. For **Pt-4**, the CIE coordinates change from (0.44, 0.18) to (0.19, 0.15). For **Pt-5** and **Pt-6**, no significant change was observed.

To study the efficiency of the triplet–triplet-energy transfer (TTET) process, which is crucial for TTA upconversion, the quenching of the triplet state of the photo-sensitizers was measured using nanosecond transient absorption (ESI†).

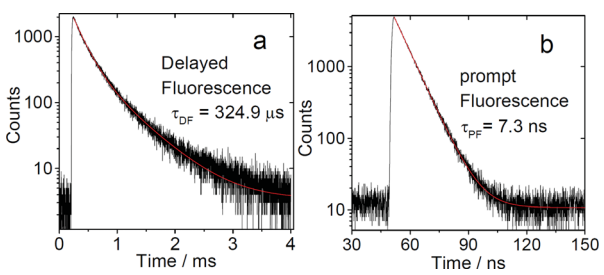


Fig. 9 Delayed fluorescence observed in the TTA upconversion with (a) **Pt-4** as the triplet photosensitizer and DPA as the triplet acceptor. Excited at 440 nm and monitored at 410 nm. (b) The prompt fluorescence decay of DPA determined in a different experiment (excited with picosecond 405 nm laser, the decay of the emission was monitored at 410 nm). $c$[DPA] = 4.0 × $10^{-5}$ M; $c$[sensitizers] = 1.0 × $10^{-5}$ M in deaerated toluene, 25 °C.

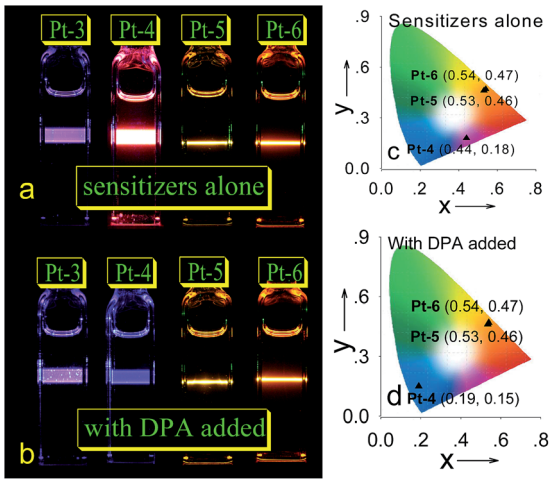


Fig. 10 Images of the emission of (a) sensitizers alone and (b) the upconversion. CIE diagram of the emission of (c) sensitizers alone and (d) in the presence of DPA (upconversion). (For **Pt-3** and **Pt-4**, $\lambda_{ex}$ = 445 nm, **Pt-5** and **Pt-6**, $\lambda_{ex}$ = 532 nm) (laser power: 5.2 mW). $c$ [sensitizer] = 1.0 × $10^{-5}$ M, $c$[DPA] = 4.0 × $10^{-5}$ M in deaerated toluene, 25 °C.

Significant quenching was observed for **Pt-4** with quenching constants of 5.65 × $10^5$ $M^{-1}$ (ESI†).

In order to unambiguously confirm that the TTA upconversion is responsible for the blue emission band of the triplet photosensitizer/DPA mixed samples, the time-resolved emission spectra (TRES) were also recorded (Fig. 11). For **Pt-4** alone, long-lived emission in the region of 631 nm was observed (Fig. 11a) with a lifetime of 55.21 μs. The difference between the lifetime values and that determined in the previous section (Table 1) is due to the fact that the background dynamics of the pulsed laser cannot be calibrated in the TRES mode. For the mixture of **Pt-4**/DPA, however, the emission band in the region 631 nm was quenched, and a new emission band in the 420 nm region developed (Fig. 11b). The lifetime of the emission was 324.9 μs. This long-lived fluorescence emission is the characteristic feature of the TTA upconversion.

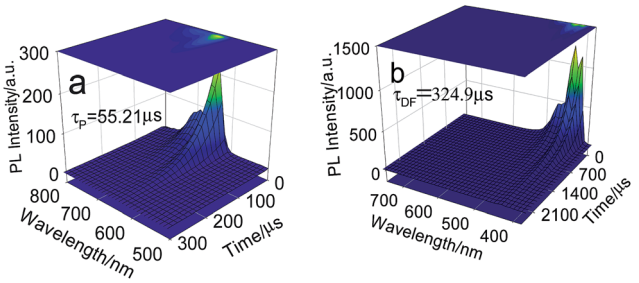


Fig. 11 Time-resolved emission spectra (TRES) of **Pt-4** alone and the TTA upconversion with the DPA as the triplet acceptor. **Pt-4** alone: (a) the phosphorescence region was measured (550–800 nm, $\tau$ = 55.2 μs) excited with nanosecond pulsed OPO laser (440 nm). TRES of **Pt-4** in the presence of DPA: (b) upconverted emission in the range of 400–500 nm was observed ($\tau$ = 324.9 μs) with nanosecond pulsed OPO laser (440 nm). $c$[DPA] = 4.0 × $10^{-5}$ M; $c$[sensitizers] = 1.0 × $10^{-5}$ M in deaerated toluene, 25 °C.

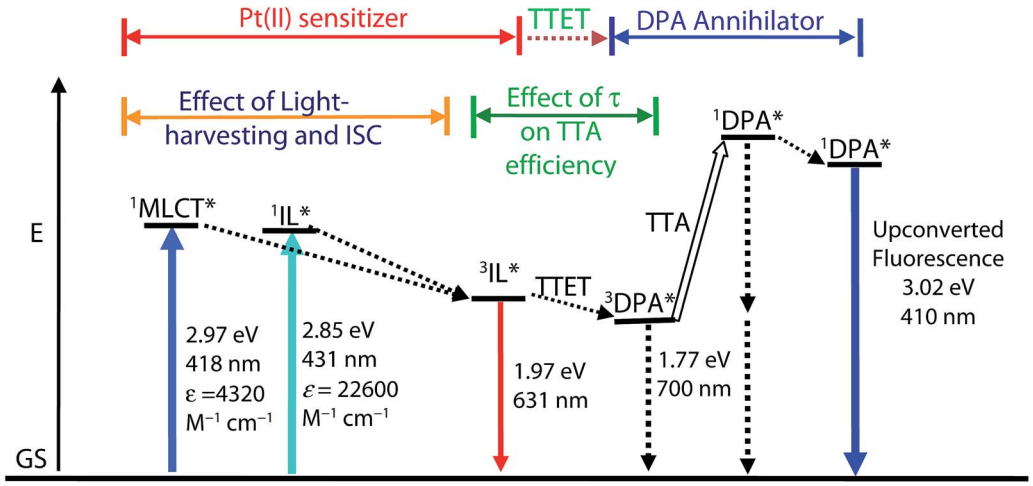


Scheme 2 Jablonski diagram of triplet–triplet-annihilation (TTA) upconversion with **Pt-4** as a triplet sensitizer (the triplet states of sensitizers are emissive) and 9,10-diphenylanthracene (DPA) was the triplet acceptor. E is energy. GS is ground state ($S_0$). $^3$IL* is intraligand triplet excited state (NI localized). TTET is triplet–triplet energy transfer. $^3$DPA* is the triplet excited state of DPA. TTA is triplet–triplet annihilation. $^1$DPA* is the singlet excited state of DPA. The emission bands observed for the sensitizers alone is the $^3$IL emissive excited state. The emission bands observed in the TTA experiment is the simultaneous $^3$IL* emission (phosphorescence) and the $^1$DPA* emission (fluorescence).

The TTA upconversion process is summarized and shown in Scheme 2. First, the singlet excited state of the triplet sensitizers are populated upon photoexcitation. Direct excitation of the ligand ($^1$IL) or $^1$MLCT will both lead to the population of singlet excited state. With the heavy atom effect of the Pt(II) atoms, the $S_1 \rightarrow T_1$ ISC leads to the $^3$IL excited state. Note that the $^3$IL excited state shows a considerably longer lifetime than the normal $^3$MLCT state. Thus the efficiency of the TTET process will be improved. Annihilation of the triplet excited state of the triplet acceptor (DPA) will produce the singlet excited state and, as a result, the singlet emission (delayed fluorescence) will be observed. The wavelength of upconverted fluorescence is shorter than the initial photo-excitation wavelength. It should be pointed out that the long-lived $^3$IL triplet excited state of **Pt-4** makes it an ideal triplet photosensitizer for triplet–triplet annihilation (TTA) upconversion.

## Conclusion

C*N^N ligands with five–six fused coordination structure and C^N^N ligands with five–five fused coordination structure were used for the preparation of six Pt(II) complexes. For each coordination profile, three different arylacetylide ligands, *i.e.* naphthalenedimide (NDI), pyrenyl (Py) and naphaleneimide (NI) acetylides, were used for the preparation of the complexes. The aim was to study the synergic effect of both the C*N^N or C^N^N ligands and the aryl acetylide ligands on the photoredox and photophysical properties of the complexes. The electrochemical properties of the complexes were studied with cyclic voltammetry, and the photophysical properties of the complexes were studied with steady-state and time-resolved absorption and emission spectroscopy. The proper formation of $^1$MLCT is the first crucial factor in the triplet photosensitizers based on transition metal complexes, which could be fine-tuned with the photoredox properties. Then, the energy level of the ligand ($^1$IL), the light harvesting antenna, at the singlet excited state should be close or higher than that of $^1$MLCT, which benefits the $^1$IL $\rightarrow$ $^1$MLCT $\rightarrow$ $^3$MLCT process. The triplet excited states are an intraligand feature and have long lifetimes (**Pt-4**, $\tau$ = 90.1 μs). The photophysical properties of the complexes were rationalized with DFT calculations. The complexes were used as triplet photosensitizers for triplet–triplet annihilation upconversion, and upconversion quantum yields up to 29.7% were observed. These results are useful for the future designing of Pt(II) complexes, which show RT phosphorescence and long-lived triplet excited states.

## Acknowledgements

We thank the NSFC (21273028, 21302224, 51172285, 21473020 and 21421005), the Royal Society (UK) and NSFC (Cost-Share-21011130154), the Program for Changjiang Scholars and Innovative Research Team in University [IRT_13R06], the Ministry of Education (SRFDP-20120041130005), Technology Program for Basic Research of Qingdao (14-2-4-47-jch), the Shandong Provincial Natural Science Foundation (ZR2013BQ028), the China Postdoctoral Science Foundation (2014M560590), the State Key Laboratory of Fine Chemicals (KF1203), and the Fundamental Research Funds for the Central Universities (DUT14ZD226, DUT2013TB07, 13CX02066A, 14CX02060A) for financial support.

## References

1 S. Chan, Y. Wang, C. Che, K. Cheung and N. Zhu, *Chem.–Eur. J.*, 2001, **7**, 4180–4190.
2 X. Wang, S. Goeb, Z. Ji, N. A. Pogulaichenko and F. N. Castellano, *Inorg. Chem.*, 2011, **50**, 705–707.

 

3 K. Lo, A. Choi and W. Law, *Dalton Trans.*, 2012, **41**, 6021–6047.
4 A. Tam and V. Yam, *Chem. Soc. Rev.*, 2013, **42**, 1540–1567.
5 E. Baggaley, J. A. Weinstein and J. Williams, *Coord. Chem. Rev.*, 2012, **256**, 1762–1785.
6 (*a*) A. Rachford, F. Hua, C. J. Adams and F. N. Castellano, *Dalton Trans.*, 2009, 3950–3954; (*b*) W. Wu, P. Yang, L. Ma, J. Lalevée and J. Zhao, *Eur. J. Inorg. Chem.*, 2012, **2**, 228–231.
7 F. Dai, H. Zhan, Q. Liu, Y. Fu, J. Li, Q. Wang, Z. Xie, L. Wang, F. Yan and W. Wong, *Chem.–Eur. J.*, 2012, **18**, 1502–1511.
8 T. N. S. Rachford and F. N. Castellano, *Coord. Chem. Rev.*, 2010, **254**, 2560–2573.
9 J. Zhao, S. Ji and H. Guo, *RSC Adv.*, 2011, **1**, 937–950.
10 P. Ceroni, *Chem.–Eur. J.*, 2011, **17**, 9560–9564.
11 Y. Ho, C. Koo, K. Wong, H. Kong, C. Chan, W. Kwok, C. Chow, M. Lam and W. Wong, *Dalton Trans.*, 2012, **41**, 1792–1800.
12 D. Ravindranathan, D. A. Vezzu, L. Bartolotti, P. D. Boyle and S. Huo, *Inorg. Chem.*, 2010, **49**, 8922–8928.
13 D. A. Vezzu, D. Ravindranathan, A. W. Garner, L. Bartolotti, M. E. Smith, P. D. Boyle and S. Huo, *Inorg. Chem.*, 2011, **50**, 8261–8273.
14 H. Guo, M. L. Muro-Small, S. Ji, J. Zhao and F. N. Castellano, *Inorg. Chem.*, 2010, **49**, 6802–6804.
15 F. N. Castellano, I. E. Pomestchenko, E. Shikhova, F. Hua, M. L. Muro-Small and N. Rajapakse, *Coord. Chem. Rev.*, 2006, **250**, 1819–1828.
16 E. O. Danilov, I. E. Pomestchenko, S. Kinayyigit, P. L. Gentili, M. Hissler, R. Ziessel and F. N. Castellano, *J. Phys. Chem. A*, 2005, **103**, 2465–2471.
17 I. E. Pomestchenko and F. N. Castellano, *J. Phys. Chem. A*, 2004, **108**, 3485–3492.
18 A. A. Rachford, S. Goeb, R. Ziessel and F. N. Castellano, *Inorg. Chem.*, 2008, **47**, 4348–4355.
19 F. Hua, S. Kinayyigit, J. R. Cable and F. N. Castellano, *Inorg. Chem.*, 2005, **44**, 471–473.
20 W. Wu, L. Liu, X. Cui, C. Zhang and J. Zhao, *Dalton Trans.*, 2013, **42**, 14374–14379.
21 S. Ji, W. Wu, J. Zhao, H. Guo and W. Wu, *Eur. J. Inorg. Chem.*, 2012, **19**, 3183–3190.
22 Y. Liu, W. Wu, J. Zhao, X. Zhang and H. Guo, *Dalton Trans.*, 2011, **40**, 9085–9089.
23 L. Huang, L. Zeng, H. Guo, W. Wu, W. Wu, S. Ji and J. Zhao, *Eur. J. Inorg. Chem.*, 2011, **29**, 4527–4533.
24 W. Wu, J. Zhao, W. Wu and Y. Chen, *J. Organomet. Chem.*, 2012, **713**, 189–196.
25 H. Sun, H. Guo, W. Wu, X. Liu and J. Zhao, *Dalton Trans.*, 2011, **40**, 7834–7841.
26 (*a*) D. Ravelli, D. Dondi, M. Fagnoni and A. Albini, *Chem. Soc. Rev.*, 2009, **38**, 1999–2011; (*b*) M. L. Marin, L. Santos-Juanes, A. Arques, A. M. Amat and M. A. Miranda, *Chem. Rev.*, 2012, **112**, 1710–1750; (*c*) W. Wu, Y. Geng, W. Fan, Z. Li, L. Zhan, X. Wu, J. Zheng, J. Zhao and M. Wu, *RSC Adv.*, 2014, **4**, 51349–51352.
27 C. F. Harris, D. A. Vezzu, L. Bartolotti, P. D. Boyle and S. Huo, *Inorg. Chem.*, 2013, **52**, 11711–11722.
28 W. Wu, D. Huang, X. Yi and J. Zhao, *Dyes Pigm.*, 2013, **96**, 220–231.
29 M. J. Frisch, G. W. Trucks, H. B. Schlegel, G. E. Scuseria, M. A. Robb, J. R. Cheeseman, G. Scalmani, V. Barone, B. Mennucci, G. A. Petersson, H. Nakatsuji, M. Caricato, X. Li, H. P. Hratchian, A. F. Izmaylov, J. Bloino, G. Zheng, J. L. Sonnenberg, M. Hada, M. Ehara, K. oyota, R. Fukuda, J. Hasegawa, M. Ishida, T. Nakajima, Y. Honda, O. Kitao, H. Nakai, T. Vreven, J. A. Montgomery Jr, J. E. Peralta, F. Ogliaro, M. Bearpark, J. J. Heyd, E. Brothers, K. N. Kudin, V. N. Staroverov, R. Kobayashi, J. Normand, K. Raghavachari, A. Rendell, J. C. Burant, S. S. Iyengar, J. Tomasi, M. Cossi, N. Rega, N. J. Millam, M. Klene, J. E. Knox, J. B. Cross, V. Bakken, C. Adamo, J. Jaramillo, R. Gomperts, R. E. Stratmann, O. Yazyev, A. J. Austin, R. Cammi, C. Pomelli, J. W. Ochterski, R. L. Martin, K. Morokuma, V. G. Zakrzewskig, G. A. Voth, P. Salvador, J. J. Dannenberg, S. Dapprich, A. D. Daniels, Ö. Farkas, J. B. Foresman, J. V. Ortiz, J. Cioslowski and D. J. Fox, *Gaussian 09 Revision A.1*, Gaussian Inc., Wallingford CT, 2009.
30 Q. Li, H. Guo, L. Ma, W. Wu, Y. Liu and J. Zhao, *J. Mater. Chem.*, 2012, **22**, 5319–5329.
31 Z. Dai, A. J. Metta-Magaña and J. E. Nuñez, *Inorg. Chem.*, 2014, **53**, 7188–7196.
32 T. Yogo, Y. Urano, Y. Ishisuka, F. Maniwa and T. Nagano, *J. Am. Chem. Soc.*, 2005, **127**, 12162–12163.
33 (*a*) X. Zhang, L. Chi, S. Ji, Y. Wu, P. Song, K. Han, H. Guo, T. D. James and J. Zhao, *J. Am. Chem. Soc.*, 2009, **131**, 17452–17463; (*b*) D. Rehm and A. Weller, *J. Chem.*, 1970, **8**, 259–271; (*c*) Z. R. Grabowski and J. Dobkowski, *Pure Appl. Chem.*, 1983, **55**, 245–252.
34 J. Zhao, W. Wu, J. Sun and S. Guo, *Chem. Soc. Rev.*, 2013, **42**, 5323–5351.
35 W. Wu, J. Zhao, H. Guo, J. Sun, S. Ji and Z. Wang, *Chem.–Eur. J.*, 2012, **18**, 1961–1968.
36 K. Hanson, A. Tamayo, V. V. Diev, M. T. Whited, P. I. Djurovich and M. E. Thompson, *Inorg. Chem.*, 2010, **49**, 6077–6084.
37 P. Yang, W. Wu, J. Zhao, D. Huang and X. Yi, *J. Mater. Chem.*, 2012, **22**, 20273–20283.
38 A. Monguzzi, R. Tubino, S. Hoseinkhani, M. Campione and F. Meinardi, *Phys. Chem. Chem. Phys.*, 2012, **14**, 4322–4332.
39 Y. C. Simon and C. Weder, *J. Mater. Chem.*, 2012, **22**, 20817–20830.
40 J. Zhao, S. Ji, W. Wu, W. Wu, H. Guo, J. Sun, H. Sun, Y. Liu, Q. Li and L. Huang, *RSC Adv.*, 2012, **2**, 1712–1728.